Control of mobile parallel manipulator
Mobil paralel manipulatör kontrolü

Berk YILDIZ[1*], Levent ÇETİN[2], Erkin GEZGİN[2]
[1]Department of Mechanical Engineering, Katip Çelebi University, İzmir, Türkiye
[2]Department of Mechatronics Engineering, Katip Çelebi University, İzmir, Türkiye
ORCIDs: 0000-0002-3236-9051, 0000-0002-7041-0529, 0000-0002-6670-9958
E-mails: b.yldz@live.com, levent.cetin@ikc.edu.tr, erkin.gezgin@ikc.edu.tr
*Corresponding author.

***Abstract*—This research article is based on the development and kinematics analysis of a novel mobile Euclidean parallel manipulator. The mobile manipulators and parallel manipulators were investigated to improve the setbacks of each of these manipulators. The design of the new mobile Euclidean parallel manipulator type robot manipulator is an improved type of both mobile platforms and parallel manipulators. The design of the mobile manipulator is created by combining the Euclidean platform with a mobile differential drive manipulator. To allow the design of this type of hybrid manipulator, the kinematics of the mobile Euclidean platform manipulator and the kinematic analysis of the new manipulator design for non-holonomic differential mobile manipulators were performed in two standalone sections. Finally, a test case study is provided in a simulation environment to validate the numerical results of the novel manipulator.**

***Keywords*—parallel manipulators; differential drives; autonomous robot; mobile parallel manipulator; hybrid robotic system.**

***Özetçe*—Bu araştırma makalesi yeni bir mobil Öklid paralel manipülatörünün geliştirilmesine ve kinematik analizine dayanmaktadır. Mobil manipülatörler ve paralel manipülatörler, bu manipülatörlerin her birinin aksaklıklarını iyileştirmek için araştırıldı. Yeni mobil Öklid paralel manipülatör tipi robot manipülatörün tasarımı, hem mobil platformların hem de paralel manipülatörlerin geliştirilmiş bir türüdür. Mobil manipülatörün tasarımı, Öklid platformunun mobil diferansiyel tahrikli manipülatörle birleştirilmesiyle oluşturulmuştur. Hibrit manipülatörün tasarımına olanak sağlamak için, mobil Öklid platform manipülatörünün kinematiği ve holonomik olmayan diferansiyel mobil manipülatörler için yeni manipülatör tasarımının kinematik analizi iki bağımsız bölümde gerçekleştirildi. Son olarak, yeni manipülatörün sayısal sonuçlarını doğrulamak için simülasyon ortamında bir test çalışması yapılmıştır.**

***Anahtar Kelimeler*—paralel manipülatörler; diferansiyel tahrik; otonom robot; mobil paralel manipülatörler; hibrit robotik sistem.**

I. INTRODUCTION

A mobile parallel manipulator(PM) has got high interest in recent years. Because of their high accuracy, velocity, stiffness, and payload capacity, the progress of parallel manipulators is accelerated since they outperform their serial counterparts [1]. However, the main drawback of PMs is their limited workspace, which restricts their applications [2]. Recently, many researchers have worked on parallel mobile robot design mechanisms [3]–[5]. Since a mobile parallel manipulator possesses the advantages of both a mobile robot and a parallel robot, it is a potential competitor in extensive applications where high accuracy operation, high rigidity, and payload capacity are required. One notable work is the Gough platform developed for use in the tire factory [6]. Later, this platform structure was generalized and widely used as the Stewart-Gough platform [6]. In the next years, there has been more interest in the analysis and synthesis of parallel manipulators [7]. Mobile robots have been used widely in such areas as automatic material handling in warehouses, transportation and health care in hospitals, and exploration in hazardous environments. Thus, as a result, there is a high interest in this area especially differential drive(DD) robots. This type of robot consists of 2 drive wheels mounted on a common axis, and each wheel can be independently driven either clockwise or counterclockwise. By varying the velocities of the two wheels, we can control the trajectories that the robot takes [8].

In this paper, we will implement a combination of a hybrid robot solution which is a mobile manipulator with a differential drive system, combined with a 3-revolute-revolute-spherical (RRS) parallel manipulator. In this research, we will utilize the Inverse kinematic analysis of a 3-RRS PM which has been performed by Li et al. [9] where the analysis is performed by using a geometrical approach. Forward kinematics of 3-PRS PM is performed by Tsai et al. [10] where he used Bezout's elimination method which is also applicable to our 3-RRS PM. Similar research has also been performed on 3-RRS parallel manipulators [11]. Then, the kinematics analysis of the combined 6 DoF manipulator is calculated. Inverse kinematics analysis of PM to be solved analytically. Forward kinematics of differential drive mobile manipulator presented as using a suggested solution by [10]. The Kinematics of the differential drive system is widely known and we will utilize the control of the DC motor with the kinematics of the DD platform [8], [12]. Finally, a numerical case study was performed as a validation action of the formulations.

II. Kinematics & Constraints of Parallel Manipulator

A. Kinematics of Mobile Parallel Manipulator

A manipulator or mechanism's displacement and variation in displacement can be investigated using a variety of techniques. While using a computer graphical approach is simple, it is not practical when the complete motion of the manipulator is taken into account. Therefore, the analytical approach is convenient to explain the whole motion of the manipulator. But, in parallel manipulators' forward kinematics case, it's very hard to compute analytically. Therefore, we will utilize Bezout's elimination method to compute forward kinematics which was used by Tsai et al [10]. The Kinematics diagram of the PM body is given in Fig. 1 and the first dyad is given in Fig. 2.

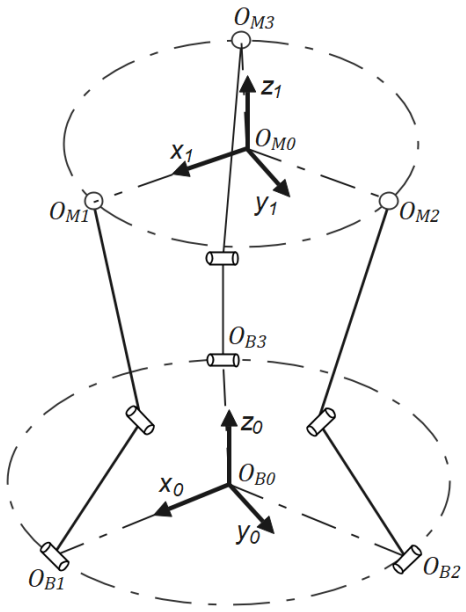

Figure 1: Kinematics model of 3-RRS Parallel Manipulator

The body of PM consists of a base which is a mobile platform but will be regarded as fixed to solve PM equations, three identical dyads, and a moveable platform. The dyads are a combination of 2 R joints with a link length of ℓ_1 and ℓ_2. Between link ℓ_2 and moveable, there is a S joint. The origin of base frame is given as O_{B_0}, and each connection point in base platform stated as O_{B_1}, O_{B_2} and O_{B_3}. The distance from base origin to revolute connection points is chosen as an equal b distance. The X_0 axis is along the vector $\vec{b_1}$ and the Z_0 axis is perpendicular to the base plane. The top moveable platforms frame is located at the center of the platform and the origin of the frame is shown as O_{M_0}. The distance to moveable platform spherical connection points are given as an equal distance of r. The X_1 axis is along $\vec{m_1}$ vector and Z_1 axis is perpendicular to platform. . In all of the dyads, the axes of the active and passive revolute joints are parallel to each other.

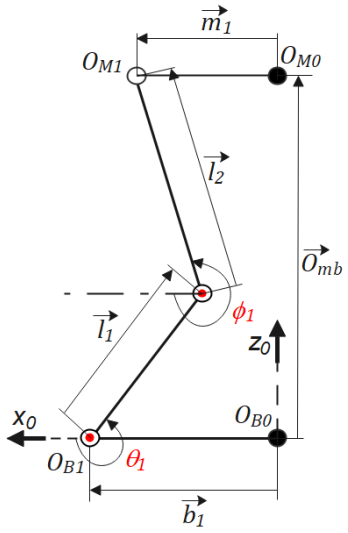

Figure 2: Kinematics model of 3-RRS Parallel Manipulator

To have an equal offset from the base frames, the connection points are positioned at the vertices of an equilateral triangle. This means that the angle between X axes of coordinate frames and each connection vector are equal to 120^o. This results, $\alpha_1 = \angle\vec{X_0}\vec{O_{B_1}} = 0°$, $\alpha_2 = \angle\vec{X_0}\vec{O_{B_2}} = 120°$, $\alpha_3 = \angle\vec{X_0}\vec{O_{B_3}} = 240°$. The manipulator is actuated by angle of rotations variables θ_1, θ_2 and θ_3 and the passive joint variables are given as ϕ_1, ϕ_2, and ϕ_3. Mobile platform kinematics will be investigated in a separate section.

B. Position Analysis of Parallel Manipulator

Each dyad is constrained to move in a plane. Constraint equations due to this planar motion are derived by Tsai et al. [1] for 3-PRS PM and these equations are valid for this type of 3-RRS PM as it's stated. To generate the rotation matrix **R** between **B** and **M** frames, *X-Y-Z* Euler rotation sequence is used. This means first a rotation around Z axis with an angle of ψ_z, then a rotation around Y axis with an angle of ψ_y, and finally a rotation around X axis with an angle of ψ_x. Then we found the matrix **R** as:

$$\mathbf{R} = \begin{bmatrix} c_y c_z & -c_y s_z & s_y \\ s_x s_y c_z + c_x s_z & c_x c_z - s_x s_y s_z & -s_x c_y \\ -c_x s_y c_z + s_x s_z & s_x c_z + c_x s_y s_z & c_x c_y \end{bmatrix} \quad (1)$$

where s and c stand for *sin* and *cos* and subscripts *x,y,z* stand for rotation angles ψ_x, ψ_y, ψ_z respectively. Only two elements of **R** are independent. In the workspace of the 3-RRS PM, the independent parameters are ψ_x and ψ_y and O_{M_z}. Position vector of the origin of the moveable platform coordinate frame represented by the base frame:

$$\vec{O_{mb}} = \begin{bmatrix} O_{M_x} & O_{M_y} & O_{M_z} \end{bmatrix}^T \quad (2)$$

O_{M1} is constrained on xz plane:

$$\vec{O_{M1}} = \begin{bmatrix} O_{M_x} + rc_yc_z \\ O_{M_y} + r(s_xs_yc_z + c_xs_z) \\ O_{M_z} + r(-c_xs_yc_z + s_xs_z) \end{bmatrix} \tag{3}$$

O_{M2} is constrained on $y = \tan(120)x$ plane:

$$\vec{O_{M2}} = \begin{bmatrix} O_{M_x} + \frac{r}{2}(-c_yc_z - \sqrt{3}c_ys_z) \\ O_{M_y} + \frac{r}{2}(-s_xs_yc_z - c_xs_z) + \sqrt{3}(c_xc_z - s_xs_ys_z) \\ O_{M_z} + \frac{r}{2}(c_xs_yc_z - s_xs_z) + \sqrt{3}(s_xc_z + c_xs_ys_z) \end{bmatrix} \tag{4}$$

O_{M3} is constrained on $y = \tan(240)x$ plane:

$$\vec{O_{M3}} = \begin{bmatrix} O_{M_x} + \frac{r}{2}(-c_yc_z + \sqrt{3}c_ys_z) \\ O_{M_y} + \frac{r}{2}(-s_xs_yc_z - c_xs_z) - \sqrt{3}(c_xc_z - s_xs_ys_z) \\ O_{M_z} + \frac{r}{2}(c_xs_yc_z - s_xs_z) - \sqrt{3}(s_xc_z + c_xs_ys_z) \end{bmatrix} \tag{5}$$

From equations (3)–(5):

$$O_{M_y} = -r(s_xs_yc_z + c_xs_z) \tag{6}$$

$$O_{M_y} = \frac{r}{2}(s_xs_yc_z + c_xs_z + 3c_ys_z) + \frac{\sqrt{3}}{2}(-2O_{M_x} - rc_xc_z + rc_yc_z + rs_xs_ys_z) \tag{7}$$

$$O_{M_y} = \frac{r}{2}(s_xs_yc_z + c_xs_z + 3c_ys_z) + \frac{\sqrt{3}}{2}(2O_{M_x} + rc_xc_z - rc_yc_z - rs_xs_ys_z) \tag{8}$$

Since equations (6) and (7) equal to each other, we can solve for the unknown ψ_z parameter. When we do the mathematical operations ψ_z results in:

$$\psi_z = \arctan(\frac{-s_xs_y}{c_xc_y}) \tag{9}$$

Then we can find the values of O_{M_x} and O_{M_y} when we register known manipulator parameters to the equations(6) and (7).

C. Inverse Kinematics of Parallel Manipulator

In this chapter, the input angles θ_1, θ_2 and θ_3 are to be found for given independent pose parameters ψ_x,ψ_y and O_{M_z} of the moveable platform. For the first dyad, the loop closure equation is:

$$\vec{O_{mb}m_1} = \vec{b_1} + \vec{\ell_1} + \vec{\ell_2} \tag{10}$$

The locations of O_{m1},O_{m2} and O_{m3} are calculated from the equations (3)–(5). Then using (10), the right side of the equation becomes:

$$x : \ell_2c\phi_1c\alpha_1 = O_{M1_x} - c\alpha_1(b + \ell_1c\theta_1)) \tag{11}$$

$$y : \ell_2c\phi_1s\alpha_1 = O_{M1_y} - s\alpha_1(b + \ell_1c\theta_1)) \tag{12}$$

$$z : \ell_2s\phi_1 = -O_{M1_z} - \ell_1c\theta_1 \tag{13}$$

By multiplying equation(11) with $c\alpha_1$, then taking the square of it and adding up with the equation(13) we can eliminate ϕ_1 from the equation. Thus, we can solve the simplified equation to find θ_1. This requires the usage of inverse functions to find values for $c\theta_1$ and $s\theta_1$. Once the input variable θ_1 is found, the passive joint angle of the dyad can be solved by inserting values to equations(11)and (13). First we find $c\phi_1$ and $s\phi_1$, then using atan2 for ϕ_1:

$$c\phi_1 = \frac{O_{M1_x} - c\alpha_1(b + \ell_1c\theta_1))}{\ell_2c\alpha_1} \tag{14}$$

$$s\phi_1 = -\frac{O_{M1_z} + \ell_1s\theta_1}{\ell_2} \tag{15}$$

$$\phi_1 = atan2(c\phi_1, s\phi_1) \tag{16}$$

The equations found are valid for all of the dyads.

To prove the inverse kinematics solution, a numerical example is to be given here. Pose parameters inputs are chosen as $O_{M_z} = 0.25m$, $\psi_x = -10°$, $\psi_y = 15°$ for the body parameters $\ell_1 = 0.147m$, $\ell_2 = 0.194m$, $b = 0.25m$, $r = 0.216m$. The formulation is then implemented into educational mathematical computation software, and an inverse kinematics solution is found. First, the task space parameters are found as $\vec{t} = \begin{bmatrix} O_{M_x} & O_{M_y} & O_{M_z} & \psi_x & \psi_y & \psi_z \end{bmatrix}^T = \begin{bmatrix} -0.002 & 0.005 & O_{M_z} & -10° & 15° & 1.32° \end{bmatrix}^T$. Then active joint variables found as $\theta_1 = (-168.91°, -36.39°), \theta_2 = (-147.99°, -45.33°), \theta_3 = (-125.60°, -71.11°)$. The passive joint variables are the obtained as $\phi_1 = (-58.73°, -146.57°), \phi_2 = (-60.39°, -132.93°), \phi_3 = (-78.06°, -118.65°)$. As our geometry constraints restrict the dyads facing outwards, the preferred set of solutions where the dyads are facing inwards is plotted in Fig. 3.

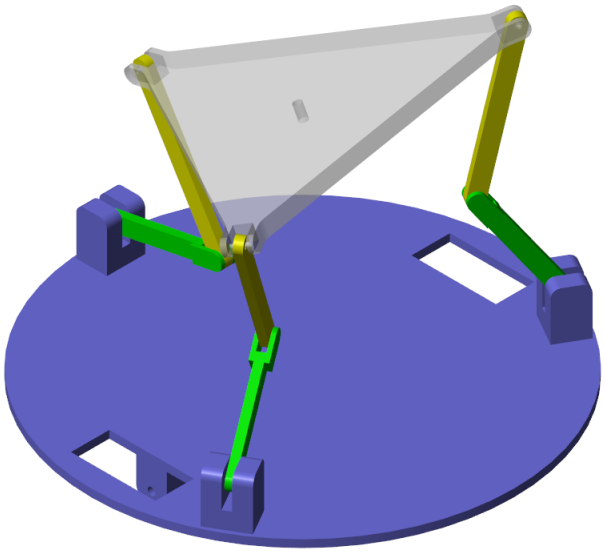

Figure 3: Inverse Kinematics Result

There are a total of 8 inverse kinematics solutions for different configurations of the dyads. Because of geometry

constraints reasons, we only used the first set of configurations for the inverse kinematics analysis.

D. Forward Kinematics of Parallel Manipulator

In this section, the pose parameters ψ_x,ψ_y and O_{M_z} of the moveable platform are to be found for given input joint variables θ_1, θ_2 and θ_3. To satisfy this, the locations of O_{M1}, O_{M2} and O_{M3} will be computed in terms of active and passive joint variables by using equation(10).

$$\vec{O_{M1}} = \vec{b_1} + \vec{\ell_1} + \vec{\ell_2} = \begin{bmatrix} c\alpha_1(b + \ell_1 c\theta_1 + \ell_2 c\phi_1) \\ s\alpha_1(b + \ell_1 c\theta_1 + \ell_2 c\phi_1) \\ -\ell_1 s\theta_1 - \ell_2 s\phi_1 \end{bmatrix} \quad (17)$$

$$\vec{O_{M2}} = \vec{b_2} + \vec{\ell_3} + \vec{\ell_4} = \begin{bmatrix} c\alpha_2(b + \ell_1 c\theta_2 + \ell_2 c\phi_2) \\ s\alpha_2(b + \ell_1 c\theta_2 + \ell_2 c\phi_2) \\ -\ell_1 s\theta_2 - \ell_2 s\phi_2 \end{bmatrix} \quad (18)$$

$$\vec{O_{M3}} = \vec{b_3} + \vec{\ell_5} + \vec{\ell_6} = \begin{bmatrix} c\alpha_3(b + \ell_1 c\theta_3 + \ell_2 c\phi_3) \\ s\alpha_3(b + \ell_1 c\theta_3 + \ell_2 c\phi_3) \\ -\ell_1 s\theta_3 - \ell_2 s\phi_3 \end{bmatrix} \quad (19)$$

Since the moveable platform has an equilateral triangle shape with a side length of $|O_{M1}O_{M2}| = |O_{M2}O_{M3}| = |O_{M3}O_{M1}| = r\sqrt{3}$:

$$\begin{aligned} &c\alpha_2(b + \ell_1 c\theta_2 + \ell_2 c\phi_2 - c\alpha_1(b + \ell_1 c\theta_1 + \ell_2 c\phi_1))^2 \\ &+s\alpha_2(b + \ell_1 c\theta_2 + \ell_2 c\phi_2 - s\alpha_1(b + \ell_1 c\theta_1 + \ell_2 c\phi_1))^2 \\ &+(-\ell_1 s\theta_2 - \ell_2 s\phi_2 - (-\ell_1 s\theta_1 - \ell_2 s\phi_1))^2 = 3r^2 \end{aligned} \quad (20)$$

$$\begin{aligned} &c\alpha_3(b + \ell_1 c\theta_3 + \ell_2 c\phi_3 - c\alpha_2(b + \ell_1 c\theta_2 + \ell_2 c\phi_2))^2 \\ &+s\alpha_3(b + \ell_1 c\theta_3 + \ell_2 c\phi_3 - s\alpha_2(b + \ell_1 c\theta_2 + \ell_2 c\phi_2))^2 \\ &+(-\ell_1 s\theta_3 - \ell_2 s\phi_3 - (-\ell_1 s\theta_2 - \ell_2 s\phi_2))^2 = 3r^2 \end{aligned} \quad (21)$$

$$\begin{aligned} &c\alpha_1(b + \ell_1 c\theta_1 + \ell_2 c\phi_1 - c\alpha_3(b + \ell_1 c\theta_3 + \ell_2 c\phi_3))^2 \\ &+s\alpha_1(b + \ell_1 c\theta_1 + \ell_2 c\phi_1 - s\alpha_3(b + \ell_1 c\theta_3 + \ell_2 c\phi_3))^2 \\ &+(-\ell_1 s\theta_1 - \ell_2 s\phi_1 - (-\ell_1 s\theta_3 - \ell_2 s\phi_3))^2 = 3r^2 \end{aligned} \quad (22)$$

By using equations(20)–(22), we rewrite them by collecting passive joint variables ϕ_1,ϕ_2,ϕ_3:

$$\begin{aligned} &h_{10} + h_{11}c\phi_1 + h_{12}c\phi_2 + h_{13}c\phi_1c\phi_2 + h_{14}s\phi_1 \\ &+h_{15}s\phi_2 + h_{16}s\phi_1s\phi_2 = 0 \end{aligned} \quad (23)$$

$$\begin{aligned} &h_{20} + h_{21}c\phi_1 + h_{22}c\phi_2 + h_{23}c\phi_1c\phi_2 + h_{24}s\phi_1 \\ &+h_{25}s\phi_2 + h_{26}s\phi_1s\phi_2 = 0 \end{aligned} \quad (24)$$

$$\begin{aligned} &h_{30} + h_{31}c\phi_1 + h_{32}c\phi_2 + h_{33}c\phi_1c\phi_2 + h_{34}s\phi_1 \\ &+h_{35}s\phi_2 + h_{36}s\phi_1s\phi_2 = 0 \end{aligned} \quad (25)$$

The three trigonometric equations(23)–(25) are nonlinear and coupled. Thus, they must be solved simultaneously to find the values of ϕ_1,ϕ_2, and ϕ_3 for given input variables. We will use Bezout's elimination method in this paper as Tsai et al. [10] did it for 3-PRS PM. Bezout's elimination method is used for reducing a set of polynomials of multiple variables into a polynomial of only one variable. To be able to apply this method, equations(23)–(25)must be transformed into polynomials. This can be done by using tangent half-angle substitution for each dyad:

$$cos\phi_1 = \frac{1 - {t_1}^2}{1 + {t_1}^2}, sin\phi_1 = \frac{2t_1}{1 + {t_1}^2} \quad (26)$$

where $t_1 = tan(\phi_1/2)$,$t_2 = tan(\phi_2/2)$,$t_3 = tan(\phi_3/2)$. This transformation is valid for all dyads. Then we can get the following equations:

$$\begin{aligned} &g_{10} + g_{11}t_2 + g_{12}{t_2}^2 + t_1(g_{13} + g_{14}t_2 + g_{13}{t_2}^2) \\ &+{t_1}^2(g_{16} + g_{11}t_2 + g_{15}{t_2}^2) = 0 \end{aligned} \quad (27)$$

$$\begin{aligned} &g_{20} + g_{21}t_3 + g_{22}{t_3}^2 + t_2(g_{23} + g_{24}t_3 + g_{23}{t_3}^2) \\ &+{t_2}^2(g_{26} + g_{21}t_3 + g_{25}{t_3}^2) = 0 \end{aligned} \quad (28)$$

$$\begin{aligned} &g_{30} + g_{33}t_3 + g_{36}{t_3}^2 + t_1(g_{31} + g_{34}t_3 + g_{31}{t_3}^2) \\ &+{t_1}^2(g_{32} + g_{33}t_3 + g_{35}{t_3}^2) = 0 \end{aligned} \quad (29)$$

We can further eliminate t_1 by using same method for equations (27)–(28):

$$\begin{vmatrix} |A_1| & |A_2| \\ |A_3| & |A_4| \end{vmatrix} = 0 \quad (30)$$

where |*| denotes the determinant of a matrix. Where A_1,A_2,A_3,A_4 as follows:

$$A_1 = \begin{vmatrix} g_{16} + g_{11}t_2 + g_{15}t_2^2 & g_{10} + g_{11}t_2 + g_{12}t_2^2 \\ g_{32} + g_{33}t_3 + g_{35}t_3^2 & g_{30} + g_{33}t_3 + g_{36}t_3^2 \end{vmatrix}$$

$$A_2 = \begin{vmatrix} g_{31} + g_{34}t_3 + g_{31}t_3^2 & g_{13} + g_{14}t_2 + g_{13}t_2^2 \\ g_{32} + g_{33}t_3 + g_{35}t_3^2 & g_{16} + g_{11}t_2 + g_{15}t_2^2 \end{vmatrix}$$

$$A_3 = \begin{vmatrix} g_{13} + g_{14}t_2 + g_{13}t_2^2 & g_{10} + g_{11}t_2 + g_{12}t_2^2 \\ g_{31} + g_{34}t_3 + g_{31}t_3^2 & g_{30} + g_{33}t_3 + g_{36}t_3^2 \end{vmatrix}$$

$$A_4 = \begin{vmatrix} g_{16} + g_{11}t_2 + g_{15}t_2^2 & g_{10} + g_{11}t_2 + g_{12}t_2^2 \\ g_{32} + g_{33}t_3 + g_{35}t_3^2 & g_{30} + g_{33}t_3 + g_{36}t_3^2 \end{vmatrix}.$$

After expanding and simplifying equation(30) transforms to:

$$j_0 + j_1t_2 + j_2t_2^2 + j_3t_2^3 + j_4t_2^4 = 0 \quad (31)$$

To further eliminate t_2 from equations (28) and (31), equation(28) written as:

$$k_0 + k_1t_2 + k_2t_2^2 = 0 \quad (32)$$

Finally, elimination method is applied again to (28) and (31) so that we can eliminate t_2:

$$\begin{vmatrix} j_3k_2 - j_4k_1 & j_2k_2 - j_4k_0 & j_1k_2 & j_0k_2 \\ j_2k_2 - j_4k_0 & j_2k_1 - j_3k_0 + j_1k_2 & j_1k_1 + j_0k_2 & j_0k_1 \\ k_2 & k_1 & k_0 & 0 \\ 0 & k_2 & k_1 & k_0 \end{vmatrix} = 0 \quad (33)$$

Expanding equation (33) results in a 16th-order polynomial with only one variable t_3. The solutions of t_3 can be obtained by solving this equation numerically. The solutions of t_1 and t_2 can be determined by substituting the found solutions of t_3 into equations (28) and (29). Although the number of the solutions is considerably large, we will show that only some solutions are feasible and the preferred solution can be determined by examining the physical constraints of the mechanism. Passive joint variables can be found from $\phi_1 = 2arctan(t_1)$, $\phi_2 = 2arctan(t_2)$, $\phi_3 = 2arctan(t_3)$.

After finding passive joint variables, we can use the equations (11)–(13)for each dyad to find O_{M_x},O_{M_y},O_{M_z} parameters. Finally, with all the known parameters, we can calculate the pose parameters psi_x,psi_y, and psi_z by using equations (3)–(5). The forward kinematics solution claimed in this chapter was proved by implementing it in educational mathematical computation software. To check both solutions of inverse and forward kinematics, the same active joint parameters and body parameters are used in the numerical calculation. The reference values of active joints are:$\theta_1 = -168.91°$, $\theta_2 = -147.99°$, $\theta_3 = -125.6°$. As stated before, there exists a maximum of 16 solutions of the polynomial given. In the numerical example, it is observed that 10 of the solutions are imaginary, hence there are 6 real solutions found. And for the values of $t_3 = -0.81, t_2 = -0.58, t_1 = -0.56$, we managed to match with the inverse kinematics solutions($O_{M_z} = 0.25m$, $\psi_x = -10°$, $\psi_y = 15°$) we have found which is shown in Fig. 4.

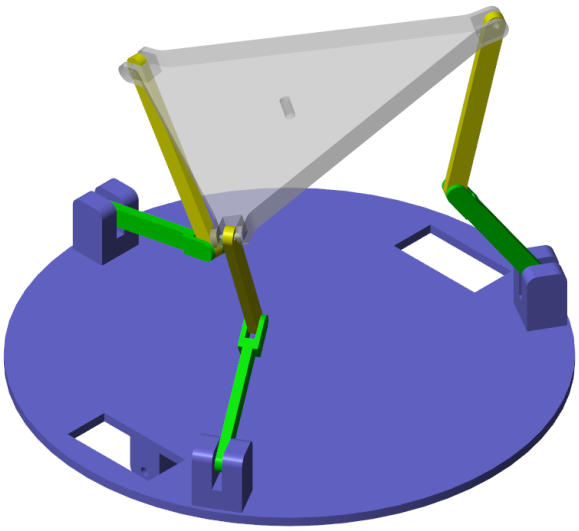

Figure 4: Forward Kinematics Result

Our design of mobile parallel manipulators simplified version is exported to Matlab Simscape environment. Then, both solutions of inverse and forward kinematics are inserted into the parameters of the mobile parallel manipulator. The Simulink model for this operation is given in Fig. 5. Fig. 3 and Fig. 4 are direct exports of this visualization model from Simscape.

III. Kinematics, Constraints & Control of Mobile Differential Drive Manipulator

In this chapter, we will investigate the mechanical constraints and kinematics of the mobile platform. Mobile platforms are frequently used for autonomous, guided, or automatic repetitive operations such as warehouse pick and place, cleaning robots, or humanoid robots with wheels. Having a mobile platform eliminates the setbacks of parallel manipulators such as workspace and mobility. Thus, we chose to use a differential drive system which is a simple and effective way of having a drive system with zero turn radius and only requires 2 motors. Our design has constraints of having 2 wheels with an axle being located at the center of the body. Then a caster to be used to balance the car and avoiding topple of whole body. We will investigate the kinematics of this system and then a control system for the manipulator with a DC drive motor to be implemented.

A. Kinematics of Mobile Manipulator

Mathematical modeling is to be generated for the DD drive mobile manipulator, and the control system is to be based on a DC motor. The primary function of the study is to give kinematics for the mobile system and do control simulations based on these formulations. As a first step, we can see the position graph of the mobile platform in Fig. 6.

B. Kinematics Modelling

First, we will investigate the mechanical behavior of the mobile system. The position of a deferentially derived mobile robot can be described by two coordinate systems, base frame and mobile platform origin frame. As it can be seen in Fig. 6, the base frame is the global frame which is the reference fixed coordinate system where the mobile platform travels. The mobile platform origin frame is the frame in motion at the center of the mobile platform. The initial location is shown as X_O,Y_O, and the mobile platform coordinate system is shown as X_r,Y_r. The origin is at the center of the wheel axle which is located at the center of the platform. These two coordinate systems can be described by using transformation matrices.

$$\dot{X}_b = R(\theta)\dot{X}_r = \begin{bmatrix} c\theta & -s\theta & 0 \\ s\theta & c\theta & 0 \\ 0 & 0 & 1 \end{bmatrix} \begin{bmatrix} \dot{x}_r & \dot{y}_r & \dot{\theta}_r \end{bmatrix} T \quad (34)$$

The mobile platform will travel straight if both wheels rotate at the same rate. If one of the wheels rotates faster than the other one, turning will happen. The mobile platform will turn to the left if the right wheel rotates faster and it will turn to the right if the left wheel rotates faster. If both wheels rotate in opposite directions at the same speed, the mobile platform will turn with zero radius at the spot. To formulate the linear speed(V) of each wheel, we will need the radius of the wheels which is denoted as r_w. We can describe the linear speed with the relation to each wheel angular speed given as ω_r(right), ω_l(left):

$$V_r = \omega_r r_w, V_l = \omega_l r_w \quad (35)$$

Then, we can calculate the velocity of the whole mobile platform by:

$$V_{mp} = V_r + V_l = \frac{r_w}{2}(\omega_r + \omega_l) \quad (36)$$

We can state that

- If the rotation speeds of the wheels are equal and the rotation directions are opposite, the mobile platform is stationary and spins in place V=0.

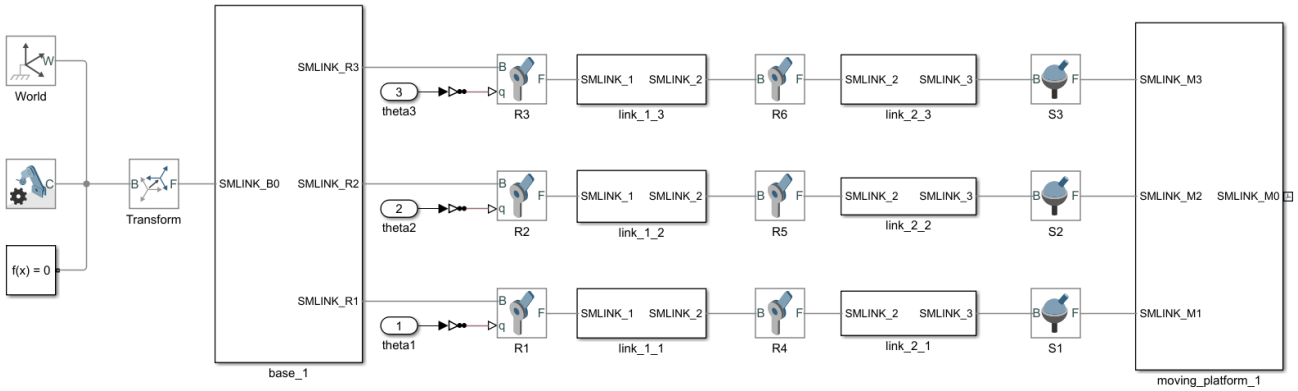

Figure 5: Simulink-Simscape model of PM

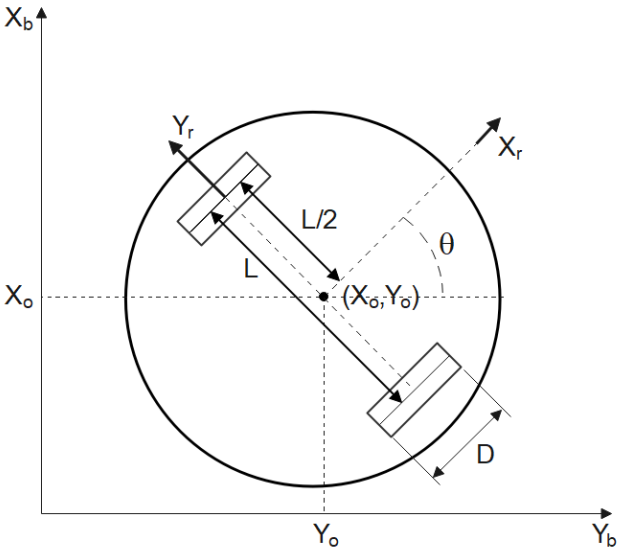

Figure 6: Position of the mobile platform

- If the rotation speeds of the wheels are equal and the rotation directions are the same, the mobile platform will travel in a straight line along $+x_r$ axis.
- If no lateral slip is assumed, then the linear velocity along y_r axis is zero.

When the right wheel rotates forward and the left wheel rests, the mobile platform rotates counterclockwise around point O with a radius of L $\omega_1 = \frac{r_w}{L}\omega_r$. When the left wheel rotates forward and the right wheel rests, the mobile platform rotates clockwise around point O with a radius of L $\omega_2 = -\frac{r_w}{L}\omega_l$. Which results angular velocity of the mobile platform as:

$$\omega_{mp} = \omega_1 + \omega_2 = \frac{r_w}{2}(\omega_r - \omega_l) \tag{37}$$

We can describe the mobile platform speed in the mobile platform frame in terms of origin point O.

$$\begin{aligned} \dot{x_O^r} &= \frac{r_w}{2}(\omega_r + \omega_l) \\ \dot{y_O^r} &= 0 \\ \dot{\theta} = \omega &= \frac{r_w}{L}(\omega_r - \omega_l) \\ \dot{q^r} &= \begin{bmatrix} \dot{x_O^r} \\ y_O^r \\ \omega \end{bmatrix} = \begin{bmatrix} \frac{r_w}{2} & \frac{r_w}{2} \\ 0 & 0 \\ \frac{r_w}{2} & \frac{-r_w}{2} \end{bmatrix} \begin{bmatrix} \omega_r \\ \omega_l \end{bmatrix} \end{aligned} \tag{38}$$

The mobile platform speed in the base frame is:

$$\begin{aligned} \dot{x_O^b} &= V cos\theta \\ \dot{y_O^b} &= V sin\theta \\ \dot{\theta} &= \omega \end{aligned} \tag{39}$$

Inserting values of V and ω from equations(36)–(37) and putting in matrix form:

$$\dot{q^b} = \begin{bmatrix} \dot{x_O^b} \\ \dot{y_O^b} \\ \omega \end{bmatrix} = \begin{bmatrix} \frac{r_w cos\theta}{2} & \frac{r_w cos\theta}{2} \\ \frac{r_w sin\theta}{2} & \frac{r_w sin\theta}{2} \\ \frac{r_w}{2} & \frac{-r_w}{2} \end{bmatrix} \begin{bmatrix} \omega_r \\ \omega_l \end{bmatrix} \tag{40}$$

Equation(40) is the kinematic model of the mobile platform. The inputs of the controller are V_r and V_l.

C. DC Motor Modelling

In many industrial applications, DC motors are used as the actuators for mobile robots and smart devices. In our application, we will use a permanent magnet-brushed DC motor(PMBDC). Control of the whole system can be based on control of the DC motor. Electrically, a PMBDC motor can be modeled with a combination of three electrical parameters such as resistor(R $Ohms$), inductor(L mH), and an input of voltage source(V). Output will be multiplied by the torque constant(K_t). Mechanically, it can be modeled with a rotating

body inertia(J kg/m^2) and a linear viscous damping component(B $N/m/s$). Then, an error will be inserted to the block with a negative sum of the back EMF constant(K_b). We will utilize Laplace transformation to get the transfer function of the PMBDC motor as illustrated in Fig. 7. The output of the block will be angular velocity(ω).

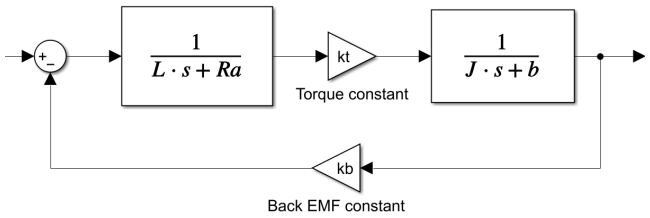

Figure 7: DC motor block diagram

We can get the linear velocity(Vmp) output by using equation(36) and output angle θ by multiplying the angular velocity output with $\frac{1}{s}$ transformation. The angular velocity of the mobile platform will be calculated by using equation(37).

D. Control System of Mobile Platform with PID Controller

Proportional-Integral-Derivative(PID) controller is an algorithm that is used to manipulate the angular velocity of DC motor in a closed loop system, with the constant gains K_p, K_D, K_I. K_p is the constant that depends on the difference between the set point and the present variable which is called the Error signal. It is the ratio that determines the ratio of output response. K_I is the constant of the integral component that sums the error signal over time. It will continuously increase over time unless it converges to zero error. K_D is the constant of the derivative component that tries to get an ideal response from the control system with an estimation of future error. This estimation requires a certain filter otherwise sensitive noises will affect the response of the system. The constant values can be found by trial and error or some of the control software such as Matlab offers tuning capabilities. The table I gives the effect and response of the system.

Constants	Rise Time	Overshoot	Settling Time	Steady-state error
K_p	Lower	Higher	Slightly higher	Lower
K_I	Slightly lower	Higher	Higher	Greatly lower
K_D	Slightly lower	Lower	Lower	Minor effect

Table I: Effects of increasing PID parameters

Modeling block diagram of PID controller given in Fig. 8.

E. Simulink Model for Mobile Platform Actuated by DC Motor with PID Control System

The Simulink model has been prepared for the DC motor with PID controller and it is given in Fig. 9. The Feedback sensor is the encoder mounted to each DC motor which is the input for the PID controller. The constant values of

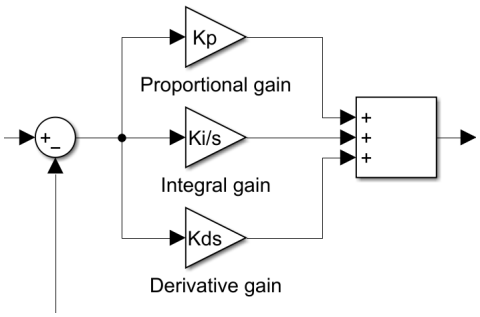

Figure 8: PID controller diagram

K_p, K_I, K_D is tuned in the Simulink environment to reach the desired linear velocity.

Then, we can conclude the model of a wheel. This is given in Fig. 10.

Based on the wheel model, we can design the control model of the whole mobile platform system in Simulink. This is given in Fig. 11.

We can also track the position and velocity of the mobile platform in the X and Y axes. The Simulink model was adjusted to give these results in a graph, shown in Fig. 12. In these graphs, we can track the position, angular velocity, and linear velocity of the mobile platform and wheels, which can be seen separately for X-Y axes.

F. Test and Simulation Result on Mobile Robot

To test the Simulink model provided, we need the specification of the DC motor. The motor used in this application is a 12V PMBDC with a gear head ratio of $n = 3$ and encoder feedback constant $Kf = 1.8$. The other parameters are shown in table II.

Parameters	Unit	Coefficient
k_t	Nm/A	0.062
k_b	v/rad/s	0.062
J_m	kg/m^2	0.0551
b_m	N m/s	0.188
R_a	Ohms	0.56
L_a	mH	0.97

Table II: 12V DC Motor parameters

The desired linear velocity(V_{mp}) of the mobile platform is 0.333 m/s. The desired angular velocity of the wheels for the wheel radius of $r = 0.05m$ is:

$$\omega_{mp} = \frac{V_{mp}}{r} = \frac{0.333m/s}{0.05m} = 1.6946rad/s \qquad (41)$$

The voltage corresponding to desired ω is $V = 12V$. Then, the next step is the tuning of the PID parameters. First, the test of the simulation model for the mobile platform is done with $K_p = 1, K_I = 0, K_D = 0$ values. The result is found as 0.08473 m/s and the plot is given in Fig. 13.

Then, we tune the PID parameters to get the desired linear velocity of mobile platform $V_{mp} = 0.333m/s$. This is done by

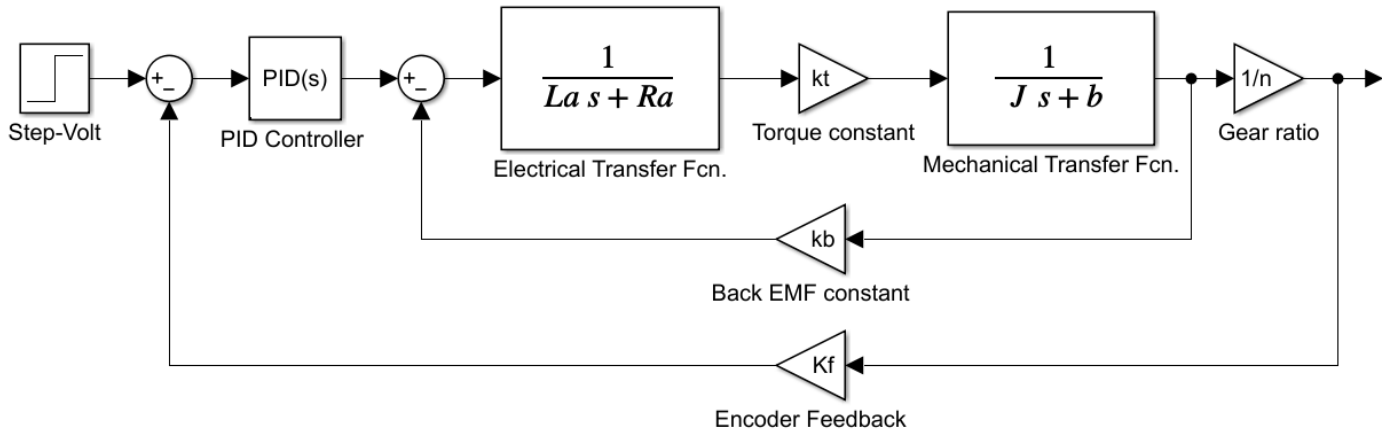

Figure 9: Model of DC Motor with PID Controller

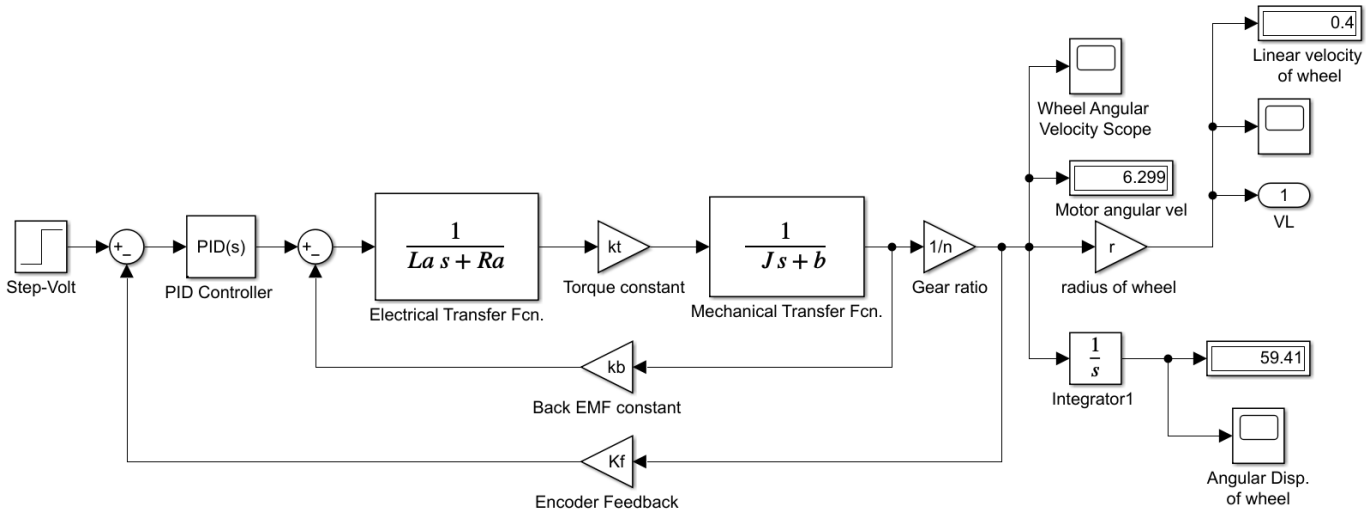

Figure 10: Complete Model of One Wheel

using Simulink PID tuning. For the values of $K_p = 6, K_I = 3, K_D = 1.5$ we get following result plot in Fig. 14:

We can find the velocity of the mobile platform along the x and y axes for the case $V_l = V_r$ as shown in Fig. 15. The Turning radius of the robot is zero.

We can find the position of the mobile platform along the x and y axes for the case $V_l = V_r$ as shown in Fig. 16.

For the case of velocity, wheels are not equal $V_r = 12V, V_l = 3V$, we can find the velocity of the mobile platform along the x and y axes as shown in Fig. 17.

For the case of velocity, wheels are not equal $V_r = 12V, V_l = 3V$, we can find the position of the mobile platform along the x and y axes as shown in Fig. 18.

Then finally, we can plot the motion parameters of the mobile platform concerning initial X and Y coordinate origins.

The linear velocity plot based on origin X-Y parameters for $V_r = 3V, V_l = 12V$ can be seen in Fig. 19. The position plot based on origin X-Y parameters for $V_r = 3V, V_l = 12V$ can be seen in Fig. 20.

IV. Conclusion

A hybrid manipulator consists of a mobile platform and a 3-RRS parallel manipulator analyzed in detail. We divided the kinematics of the whole system into 2 sections which dealt with the kinematics problem of the 3-RRS parallel manipulator and the kinematics of the differential drive mobile platform. We provided a formulation for forward and inverse kinematics of PM. and we proved it with a numerical case study done in educational software and the final pose of the PM plotted

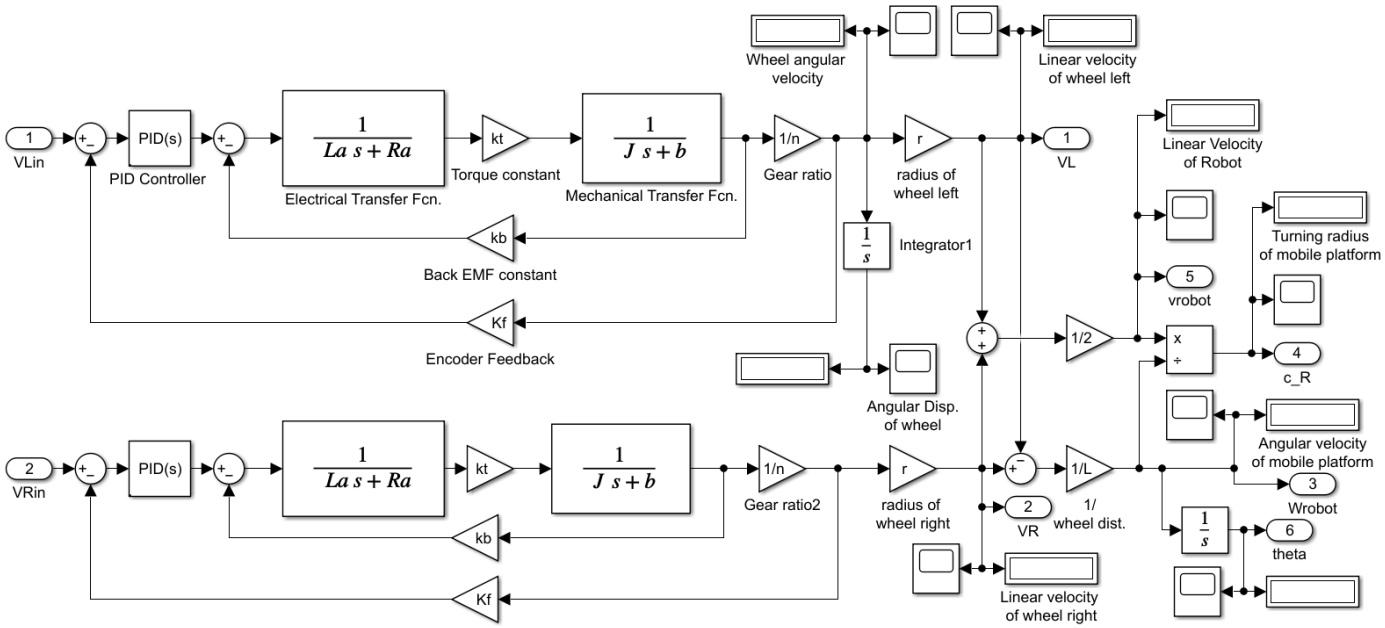

Figure 11: Simulink model of mobile platform system

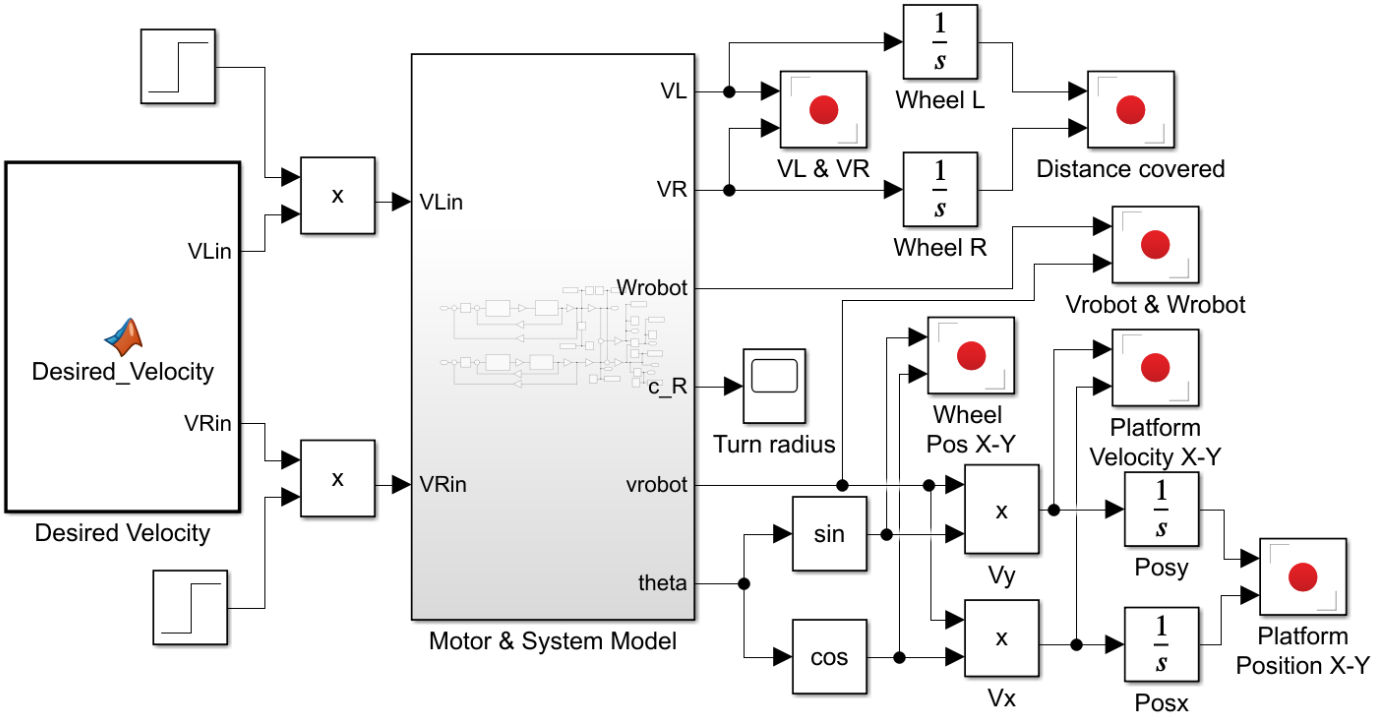

Figure 12: Complete Simulink model of mobile platform system with options of plotting graphs

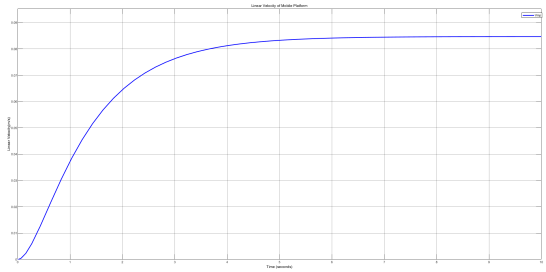

Figure 13: Simulink results of system for $K_p = 1, K_I = 0, K_D = 0$

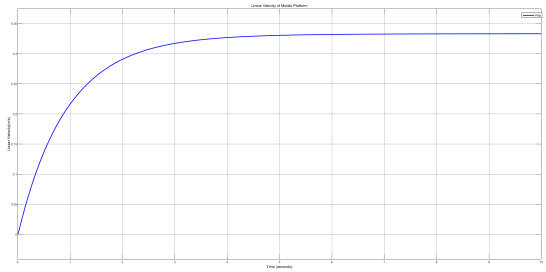

Figure 14: Simulink results of system for $K_p = 6, K_I = 3, K_D = 1.5$

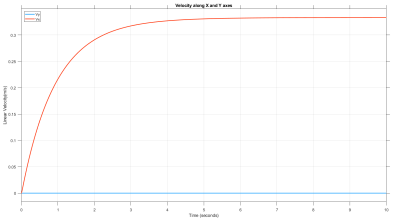

Figure 15: Simulink results of velocity along x and y direction

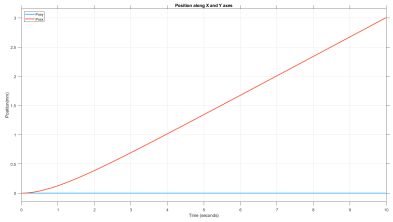

Figure 16: Simulink results of position along x and y direction

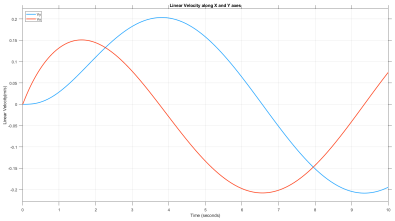

Figure 17: Simulink results of velocity along x and y direction

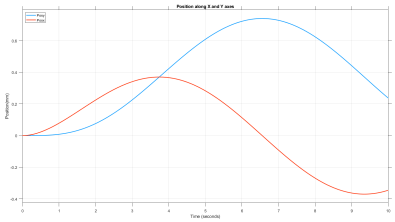

Figure 18: Simulink results of position along x and y direction

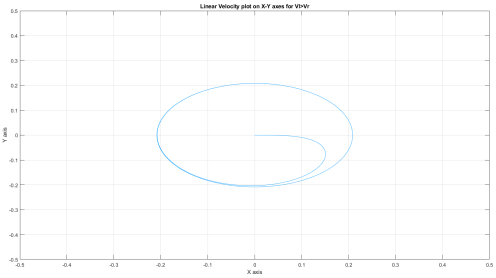

Figure 19: Simulink results of velocity based on origin(X-Y)

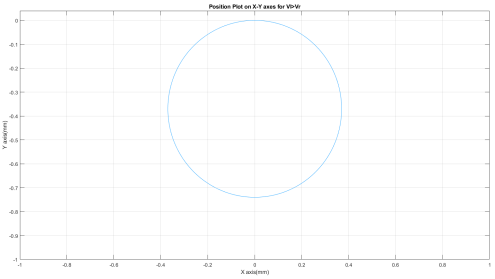

Figure 20: Simulink results of position based on origin(X-Y)

in the Matlab Simscape environment. Then, we described the kinematics formulation of a non-holonomic differential drive mobile platform. Together with DC motor control theory, we implemented a PID controller to improve the system response of the mobile platform. Simulink results are shown in graphs as shown in Fig. 19 and Fig. 20. Based on these results, we conclude that the system-based model of differential drive mobile can be solved and a mobile platform can be combined with a parallel manipulator to solve industrial or daily life tasks and improve the abilities of a single robot. The outputs of this research paper will be used in developing a hybrid mobile parallel manipulator system.

AUTHOR CONTRIBUTIONS

This paper is a part of *Berk Yıldız*'s MSc. thesis. *Prof. Dr. Levent Cetin* is the advisor and *Assoc. Prof. Dr. Erkin Gezgin* is the co-advisor of this thesis. All authors equally contributed to writing the paper.

ACKNOWLEDGEMENTS

We would like to acknowledge Dr. Fatih Cemal Can for his contribution to the research.

REFERENCES

[1] Tsai LW. Robot Analysis and Design: The Mechanics of Serial and Parallel Manipulators, 1999, John Wiley and Sons, Inc., USA.

[2] Tsai LW. Systematic Enumeration of Parallel Manipulators. In: Boer CR, Molinari-Tosatti L, Smith KS (eds). Parallel Kinematic Machines. Advanced Manufacturing. 1999, Springer, London, pp. 33-49.

[3] Gough E. Contribution to Discussion of Papers on Research in Automobile Stability, Control and Tyre Performance. In Proceedings of the Institution of Mechanical Engineers: Automobile Division, pp. 392–394, 1956.

[4] Guzin D, Gezgin E. Development of a robot manipulator design for brain surgery. Journal of Intelligent Systems with Applications 2020; 3(1): 48-51.

[5] Ozbek S, Gezgin E, Yazici MV. Design of soft fingers for a surgical robotic hand with hybrid structure. Journal of Intelligent Systems with Applications 2021; 4(1): 38-41.

[6] Stewart D. A platform with six degrees of freedom. Proc. Inst. Mech. Eng. 1965; 180(1): 371–386.

[7] Can FC, Alizade R. Analysis and Synthesis of Parallel Manipulators. PhD Dissertation, 2008, Izmir Institute of Technology, Turkey.

[8] Dudek G, Jenkin M. Differential Drive Kinematics. Computational Principles of Mobile Robotics, 2nd. ed., Cambridge University Press, USA, 2010, pp. 39-47.

[9] Li Y, Xu Q, Yugang Liu. Novel design and modeling of a mobile parallel manipulator. In Proceedings 2006 IEEE International Conference on Robotics and Automation, 2006. ICRA 2006., Orlando, FL, USA, 2006, pp. 1135-1140.

[10] Tsai M, Shiau TN, Tsai Y, Chang TH. Direct kinematic analysis of a 3-PRS parallel mechanism. Mechanism and Machine Theory 2003; 38(1): 71-83.

[11] Tetik H. Modelling and control of a 3-RRS parallel manipulator, 2016, Izmir Institute of Technology, Turkey.

[12] Hirpo BD, Zhongmin W. Design and Control for Differential Drive Mobile Robot. International Journal of Engineering Research and Technology 2017; 06(10): 327-334.